ACS Photonics

pubs.acs.org/journal/apchd5

Article

Efficient Integrated Amplifier-Assisted Laser on Erbium-Doped Lithium Niobate

Jiangwei Wu,[†] Xiongshuo Yan,[†] Xueyi Wang, Tingge Yuan, Chengyu Chen, Hao Li, Yuping Chen,* and Xianfeng Chen

Cite This: *ACS Photonics* 2024, 11, 2114–2122

Read Online

ACCESS | Metrics & More | Article Recommendations | Supporting Information

ABSTRACT: A light source is an indispensable component in on-chip systems. Compared with hybrid or heterogeneous integrated laser, monolithically integrated laser is more suitable for high-density photonic integrated circuits because of the capability of large-scale manufacturing, lower active-passive coupling loss, and less test complexity. Recent years have seen the spark of research on the rare-earth ion-doped thin film lithium niobate, and demonstrations have been made in both classical and quantum chips. However, low output power and limited quantum emitting efficiency hinder the application of the chip-scale laser source based on this platform. Here a highly efficient integrated laser assisted by an amplifier is proposed and experimentally prepared on Erbium-doped thin film lithium niobate. A slope efficiency of 0.43% and a linewidth of 47.86 kHz are obtained. The maximum integrated laser power is 7.989 μW. Our results show a viable solution to improve efficiency without changing the intrinsic quantum emitting efficiency of the material, and our design has potential applications in being incorporated with functional devices such as optical communications, integrated quantum memory, and quantum emission.

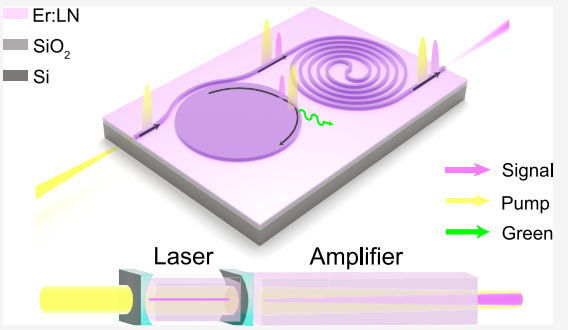

KEYWORDS: *integrated photonics, lithium niobate, Erbium ion, optical microcavity, laser, pump efficiency*

INTRODUCTION

Integration is of great significance in device miniaturization and energy efficiency improvement.[1] Photonic integrated circuits (PICs) as one of the important goals for the development of photonics have attracted enormous attention and have become one of the most investigated research fields. The light source is the heart of the optical system and the beginning of any optical application.[2−7] Many solutions for lasers have been provided. The requirements of ideal chip-scale lasers include sufficient large power with high power efficiency, continuous-wave emission in fiber-based communication bands, compatibility with CMOS (complementary metal oxide semiconductor) processes, and so on.[8] Taking silicon-based PIC as an example, Group III−V lasers have been commercialized for a long time and have been explored extensively to combine with silicon photonics using hybrid and heterogeneous integration.[9−14] Meanwhile, silicon-based Raman lasers,[15] silicon quantum dots lasers,[16] and other Group IV lasers that could be monolithically integrated with silicon photonics are attracting researchers' attention.

Lithium niobate (LN) is another emerging integrated photonic platform material. It has been widely used in optical and microwave fields due to its rich properties such as wide transparent wavelength range, excellent electro-optic and acousto-optic characteristics, and large second-order nonlinear susceptibility.[17] In particular, since the thin film LN (TFLN) has been commercially available, many compact and low-cost photonic devices with high performance can be achieved on this platform,[18−20] such as efficient frequency convertors,[21−26] electro-optical modulators,[27−30] acousto-optic modulators,[31] frequency comb sources,[32−34] and sensors.[35,36] As for an integrated laser on LN, solutions are limited. Considering the stringent requirements, on-chip lasers based on LN await further investigation. The hybrid integrated electrical pumped laser with TFLN has been demonstrated.[37] However, a monolithically integrated laser is preferred because of the capability of large-scale manufacturing, lower active-passive coupling loss, and less test complexity. Doping rare earth ions into LN crystal could make it a gain medium, which has been performed on many materials such as silica fiber, silicon nitride, and yttrium aluminum garnet.[38−44] With doped TFLN, a monolithically integrated laser is now possible. We developed an Erbium (Er)-doped TFLN and fabricated a microdisk laser in 2021.[45] Rare-earth ion-doped TFLN has been considered a promising material platform for both classical and quantum-

Received: March 2, 2024
Revised: April 4, 2024
Accepted: April 4, 2024
Published: April 18, 2024

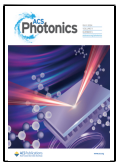

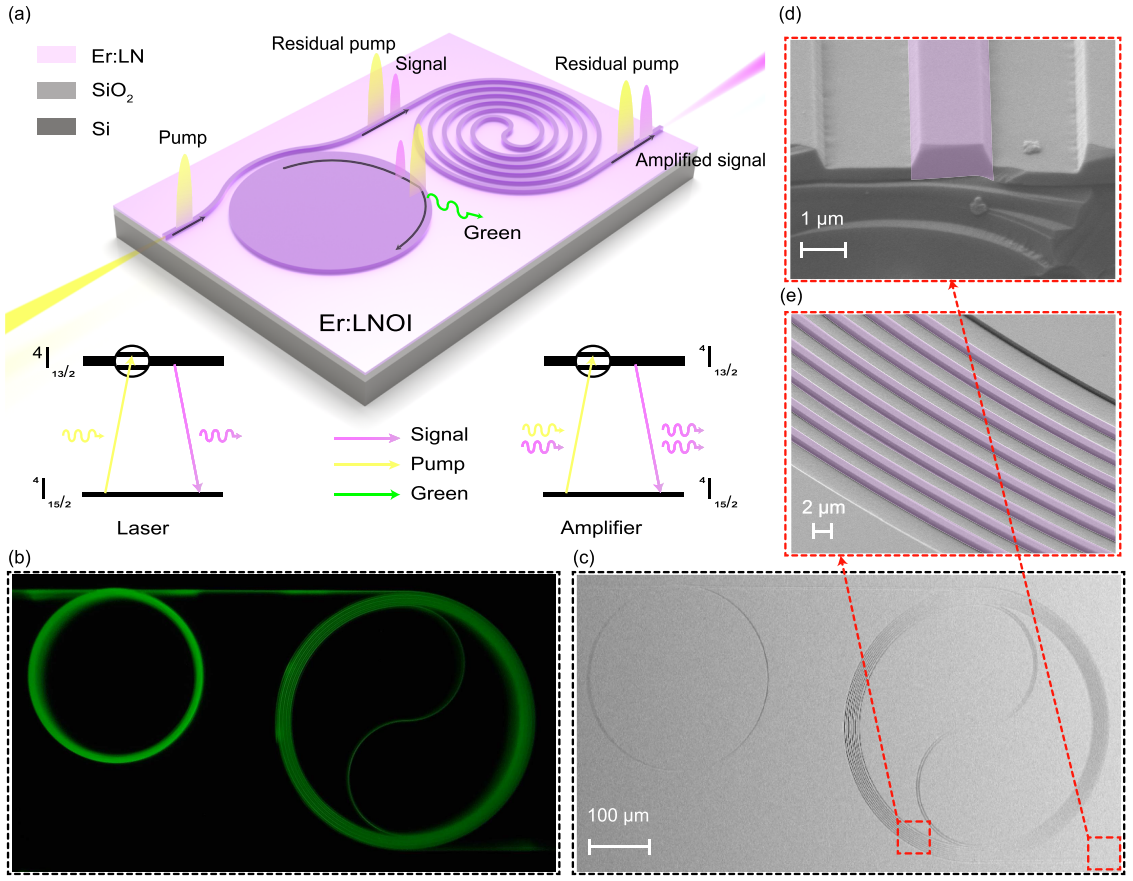

Figure 1. Concept and structure of the IAL. (a) Schematic of the IAL. (b) Microscopic images of the IAL with pump. (c–e) Scanning electron microscopy images of the IAL; zoomed-in figures are the edge coupler and waveguide of amplifier.

integrated photonics.[46,47] In recent years, many active devices for classical application including microdisk laser, microring laser, single-mode laser, and waveguide amplifiers were reported on this platform.[45,48−69] Quantum applications like single photon sources and quantum memory have also been demonstrated.[70−72]

The laser transition of trivalent Er ions matches the C-band telecom window, making it the most attractive dopant ion for photonic application. As for the Er-doped on-chip laser, the output laser powers of most existing results are too small to support subsequent work, and their slope efficiencies are low ($\sim 10^{-4}$), so the pump powers have to be large. We propose and experimentally demonstrate an efficient integrated amplifier-assisted laser (IAL) on an Er-doped TFLN, which consists of a microdisk resonator and a spiral waveguide in a relatively small footprint ($\sim$0.405 mm^2). A maximum on-chip laser power of 7.989 μW (at 1531.6 nm) is achieved under a nontunable pump, while with a tunable pump source, the IAL could emit 7.26 μW-laser with a slope efficiency of 4.3×10^{-3}, and laser linewidth is 47.86 kHz. We also examine the thermal tunability of the device. The numerical simulation is given, and it fits well with the experimental data. The IAL would be a possible solution for an efficient monolithically integrated light source in large-scale PIC and enable more types of quantum applications.[73−76]

RESULTS

The structure of IAL is shown in Figure 1a. When the pump laser is injected in the waveguide through an edge coupler and coupled into the microdisk resonator, the Er ions in the whispering-gallery-mode (WGM) cavity would be excited to higher states ($^4I_{11/2}$ with 980 nm pump, $^4I_{13/2}$ with 1480 nm pump), thanks to the enhanced light−matter interaction. After a rapid nonradiation decay, they would emit C-band laser signals. As the signal laser and residual pump laser couple back and propagate along the spiral waveguide amplifier, the pump laser excites the Er ions and builds up population inversion. The signal laser from the microdisk would be amplified, and the energy of the pump laser is further transferred into the signal laser. The energy level diagrams included in Figure 1a plot the lasing and amplification processes. It is worth noting that the cooperation upconversion of Er ions under a pump would also generate a green light. This process is detrimental to the quantum emitting efficiency of the C-band laser, while it could help us to estimate the power density of the pump laser. Figure 1b shows the microscopic images of the device with the pump on. The green emission highlights the microdisk cavity and the spiral waveguide, where the enhancement of light−matter interaction in the resonator is obvious.

The scanning electron microscopy image of the device and zoomed-in figures of the edge coupler and spiral waveguides (with false color) are shown in Figure 1c–e. As the linewidth of the available nontunable pump is about 1 nm, we chose a 300-μm-diameter microdisk as the laser resonator, so that the FSR (free spectral range) of the cavity is small enough for the pump laser to couple into. The width of the waveguide is set as 1 μm for single-mode propagation, and the microdisk-waveguide coupling region is adiabatically tapered to 0.6 μm

https://doi.org/10.1021/acsphotonics.4c00391
ACS Photonics 2024, 11, 2114−2122

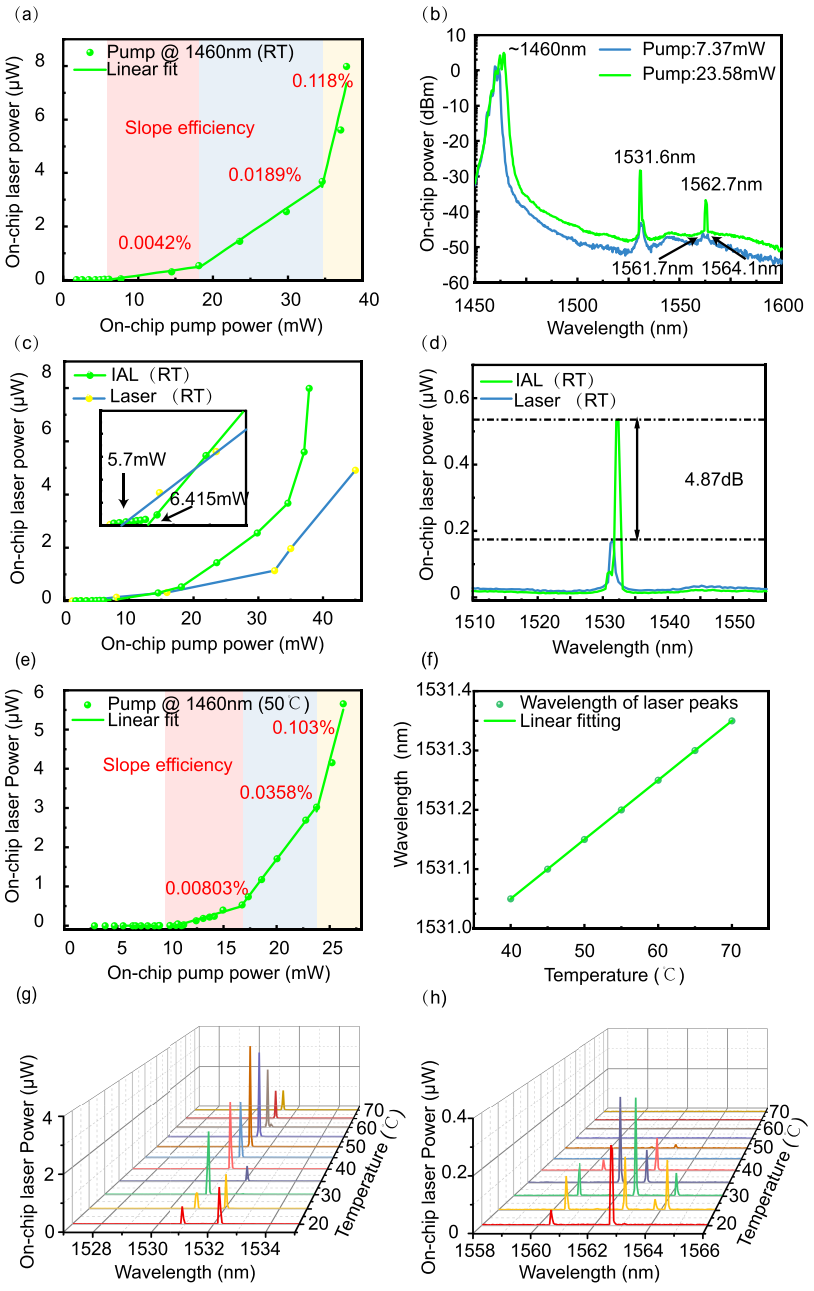

Figure 2. Performance under a nontunable pump. Emission power at 1531.6 nm (a) and spectra (b) of the IAL under a nontunable pump. (c) Emission power comparison between the microdisk laser and IAL; the inset shows the details about the laser threshold. (d) Laser peaks comparison between the microdisk laser and IAL with the same nontunable pump at 17.98 mW. (e) Emission power at 1531.6 nm of the IAL at 50 °C. (f) Wavelength drift of laser peaks versus different temperatures (from 40 to 70 °C). Evolution of laser mode around 1530 nm (g) and 1562 nm (h) with temperature increasing from 20 to 70 °C.

for evanescent coupling. As for the spiral waveguide, the minimum bending radius is 100 μm to reduce scattering loss, and the gap between two adjacent waveguides is 2 μm to avoid crosstalk. The whole device had a footprint of ~0.405 mm^2.

The IAL is first pumped by a nontunable laser (1460 nm LD light source, Golight Co., Ltd.), whose center wavelength is around 1460 nm. To compare the device with a single microdisk laser and single spiral amplifier, we use on-chip power in this essay to eliminate the effect of coupling difference. The performances are illustrated in Figure 2. The relation between the laser and pump power is shown in Figure 2a. The laser power increases with enlarged pump power in a changing slope efficiency, as shown in differently colored blocks in Figure 2a. The nonuniform efficiency could also be seen in a single microdisk laser. When coupled pump power just exceeds the laser threshold in the cavity, the ground state absorption (GSA) dominates in the following waveguide region, and the laser would experience large absorption loss before being coupled to the fiber. As the pump further increases, more Er ions could be excited, so the spiral waveguide becomes gainful. The maximum slope efficiency of 0.118% is achieved when the gain of the amplifier is saturated; meanwhile, a maximum on-chip laser power as high as 7.989 μW is observed. (The detailed characterizations of single microdisk laser and single spiral amplifier are shown in the Supporting Information.) Apart from the signal around 1531

https://doi.org/10.1021/acsphotonics.4c00391
ACS Photonics 2024, 11, 2114−2122

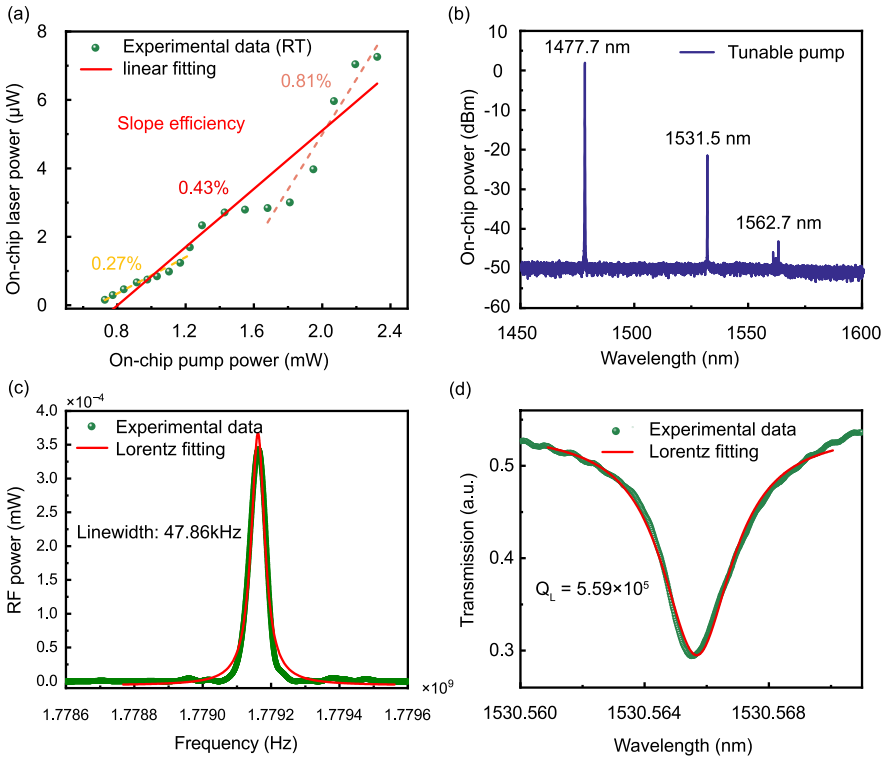

Figure 3. Performance under tunable pump. (a) Relationship between laser power and tunable pump power. (b) The collected spectrum of the IAL under tunable pump. (c) The linewidth of the signal laser. (d) Lorentzian fitting of a measured mode around 1530.56 nm exhibiting a loaded Q factor of 5.59×10^5.

nm, a laser around 1562 nm could also be generated since the microdisk cavity supports multimode laser emission. Figure 2b shows the collected spectra covering both pump and main laser wavelengths with different pump power; the multiple peaks around 1562 nm also denote multimode emission.

The lasing performance of the IAL is compared with that of the single microdisk laser in Figure 2c. The two devices are fabricated on the same chip simultaneously, and the microdisk cavities share the same geometrical parameters including microdisk resonator radius and the coupling gap with the bus waveguide. The coupling loss caused by the edge coupler is excluded to get an on-chip pump power. The IAL possesses a larger threshold power of 6.415 mW (inset of Figure 2c) because a longer waveguide with a larger GSA needs more pump power to be transparent for laser signals to output, so the slope efficiency of the microdisk laser is slightly larger than that of IAL with small pump power, and soon be surpassed with increased pump power. While the two devices are under the same on-chip pump power of 18 mW, we achieve a laser intensity enhancement of 4.87 dB as shown in Figure 2d. The mismatch of the two signal peaks might be due to the size deviation of the cavity caused by fabrication error, so they support shifted resonances. These results suggest that the IAL exhibits superior laser output performance to a single microdisk laser and thus could be a better candidate for on-chip integration.

We also examine the performance of the IAL at different temperatures to prove its stability under various conditions and thermal tunability. Figure 2e shows that the IAL behaves similarly at 50 °C as that at room temperature. There is no significant difference in its slope efficiency and the maximum on-chip laser power at different temperatures. The signal peaks are shifting with the temperature changing from 40 to 70 °C, as shown in Figure 2f, indicating a thermal tuning coefficient of 10 pm/°C. It is worth noting that the mode evolution at the two main lasing bands (around 1531 and around 1562 nm) with temperature increase could be observed in Figure 2g, h. Apart from the thermal tuning effect, multimode lasing becomes single-mode lasing (around 1531 nm) when the chip is heated. The multimode lasing at around 1562 nm is suppressed at high temperatures (>50 °C). We could also find that the laser peaks around 1531 nm increase with the temperature and then decrease. These phenomena are caused by the overlap shifting of cavity resonance and the gain profile of the Er ions. It also provides a potential degree of freedom to manipulate the device. To prove the origin of the thermal evolution, please find the detailed analysis in the Supporting Information.

Compared with a nontunable laser, a tunable laser is more expensive and often with a larger volume. However, the narrow linewidth laser emission and tunability would help examine the optimum performance of the IAL. We use a tunable 1480 nm laser (Toptica CTL 1500) as the pump and obtain the light-in-light-out (L-L) relation as shown in Figure 3a. The wavelength of pump lasers is tuned to achieve the best coupling and oscillating conditions. The multimode laser competition and the cavity resonance shifting caused by the heating of light absorption might be detrimental to laser power, especially when the pump power is small. Therefore, there is a fluctuation of signal laser power in the L-L relation. With a large pump, the signal power would be amplified in the spiral waveguide and would increase with less fluctuation until the pump is saturated. The situation is better under nontunable pumps as shown in Figure 2a, e. Since the needed pump power is larger to generate the same signal laser, the residual pump is larger for amplification. The behavior of changing slope efficiency is

https://doi.org/10.1021/acsphotonics.4c00391
ACS Photonics 2024, 11, 2114−2122

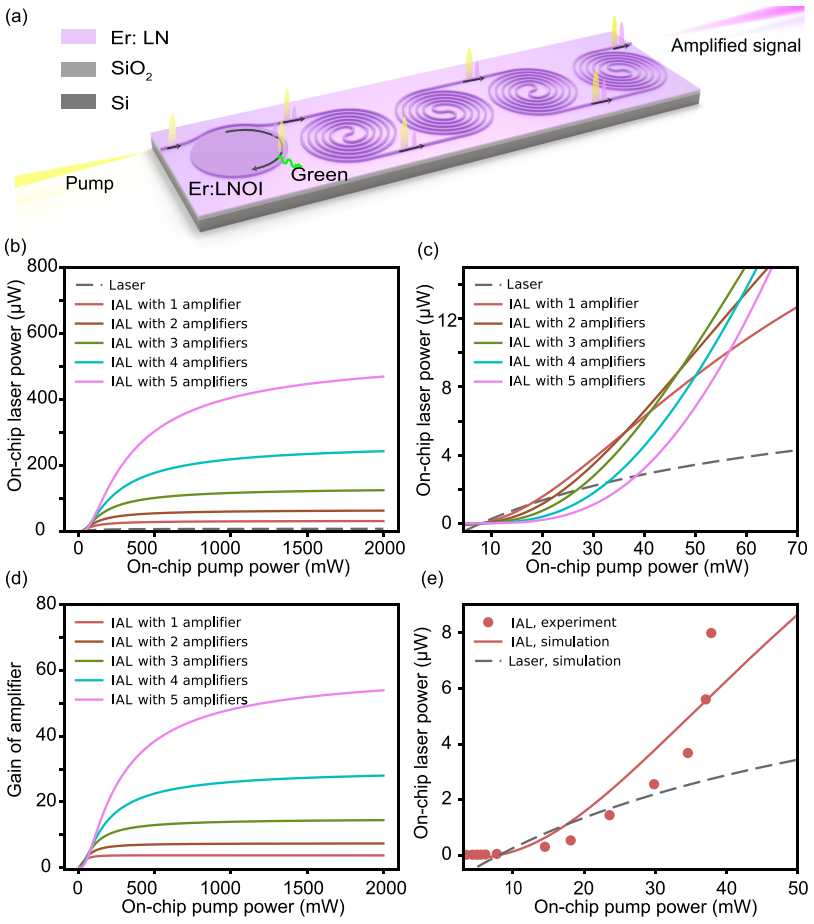

Figure 4. Numerical simulation. (a) Schematic of the cascaded IAL. (b) Simulated laser power from the cascaded IAL with different numbers of spiral waveguide amplifiers. (c) Zoomed-in figure of (b). (d) Gain of the amplifier in the cascaded IAL. (e) Comparison of the simulation and experiment results of the IAL.

similar to that under nontunable pumps. The average slope efficiency is 0.43%, while in some regions, as fitted with yellow and pink dashed lines, the slope efficiencies are 0.27 and 0.81%, respectively. The maximum laser power is 7.26 μW, slightly lower than that with a nontunable pump since the pump power is limited. The higher efficiency is easy to explain. Figure 3b shows the collected spectrum covering both pump and main laser wavelengths. Compared with a nontunable pump laser (shown in Figure 2b), the linewidth of a tunable pump laser is quite narrow; thus, the power needed to excite the Er ions is reduced. The lowered pump power makes it easier to perform a linewidth measurement. We use the double beam heterodyne method, and the experimental setup is shown in Figure S5 in the Supporting Information. The output of the IAL is combined with another C-band tunable laser (Toptica CTL 1550). The linewidth of the reference laser is around 1 kHz, and its power is attenuated to the microwatts level. The combined signal is sent to a photodetector and then to the electrical spectrum analyzer (ESA). By tuning the reference laser, the beat note signal is obtained. Since the linewidth of IAL is much larger than that of the reference, the Lorentz fitted linewidth is approximately equal to the linewidth of IAL. The linewidth of the output laser at 1531.5 nm is 47.86 kHz, as shown in Figure 3c.

The propagation loss is derived by evaluating the intrinsic Q of a simultaneously fabricated microring with a 200-μm radius, which is similar to that of the spiral waveguide. The resonance at around 1531 nm is shown in Figure 3d with a loaded Q factor of 5.59×10^5, and the calculated intrinsic Q is 6.24×10^5. The propagation loss α is calculated by

$$\alpha = \frac{2\pi N_{\text{eff}}}{\lambda_0 Q_{\text{i}}} \tag{1}$$

where N_{eff} is the effective refractive index of the waveguide at the wavelength λ_0. The obtained propagation loss around 1531 nm is 0.53 dB/cm, and it is then used to estimate the gain performance of the IAL.

DISCUSSION

The gain saturation of the amplifier limits the maximum on-chip laser power. For a waveguide amplifier, the gain saturation is mainly caused by the pump absorption saturation of the Er ions. Increasing the doping concentration of Er ions might achieve higher gain, while the energy-transfer upconversion among neighboring Er ions and fast quenching would be severe with a high Er concentration, which would lower the pump efficiency. Prolonging the waveguide might be a safer solution for a high-power laser output.

Figure 4a illustrates the IAL with multiple spiral waveguides, i.e., cascaded IAL, which could increase the length of the amplifier while keeping the footprint reasonably small. We perform a numerical simulation to predict the maximum laser output of a cascaded IAL, and the results are shown in Figure 4b,c. The dashed line denotes the simulated microcavity laser

https://doi.org/10.1021/acsphotonics.4c00391
ACS Photonics 2024, 11, 2114−2122

output, which is set as the signal laser in the calculation of the cascaded IAL output. When the pump power is far larger than the threshold, the approximation of uniform excitation along the waveguide is taken, and gain coefficient behavior with a large signal and under large pump power is considered in the calculation. As the number of spiral amplifiers increased, the threshold would increase, and the maximum output laser power is increased. Maximum laser output in the order of one hundred microwatts could be achieved in the IAL with 5 cascaded spiral waveguides, while larger pump power is needed to compensate for the increased loss, as shown in Figure 4c. The gain of the amplifier, G, is defined as

$$G = \exp[(g + \alpha)l] \tag{2}$$

where

$$g \propto \frac{g_0}{\left[1 + \frac{I_{psa(l)}}{I_p}\right]\left(1 + \frac{I_l}{I_{ls}}\right)} \tag{3}$$

α is the loss of the amplifier, and l is the length of the amplifier. g_0 is the gain coefficient of the amplifier with a small signal, I_p is the pump power, and $I_{psa(l)}$ is the saturated pump power of the amplifier, which depends on the length of the waveguide. I_l and I_{ls} are the laser output of the microcavity and the saturated laser power, respectively. Figure 4d shows the relationship between pump power and the gain of the amplifier, where the saturation occurs in a high pump. The experimental result fits well with the simulation as shown in Figure 4e, and minor deviation might come from the power-dependent loss coefficient.

The polarization of the applied pump laser has an apparent influence on the signal laser both in power and wavelength. The mode-field-matching condition between the lens fiber and the edge coupler accounts for the coupling loss of the pump laser and consequently the on-chip pump laser power. For a single-mode ridge waveguide, the mode distributions of TE and TM modes are different, and thus, the coupling efficiency with lens fiber varies. On the other hand, since LN is an anisotropic material, the absorption and emission cross sections of the doped Er ions are polarization-dependent.[77] In our experimental setup, a polarization controller is used to change the applied polarization of the pump laser to ensure the largest laser output. The mode competition of the output signal laser at the telecommunication band is observed with different polarizations. A detailed discussion can be found in the Supporting Information.

The mode splitting and mode competition could be seen throughout the experiment, which are detrimental to high-slope efficiency and single-mode laser output. The high-power pump laser in the cavity would couple with high-order modes, hindering the continuous increase of fundamental mode power. The single-mode laser output with good monochromaticity, high stability, and good beam quality is preferred in a PIC. To this end, many methods can be utilized. For example, replacing the microdisk cavity with a microring of a proper width could give a single transverse mode. Furthermore, a smaller radius brings a larger FSR to reduce the longitudinal modes at the target wavelength band. The Vernier effect in which two coupled cavities with different FSRs could also achieve a single-mode laser. Besides, the thermal effect of the device shows another method to obtain single-mode emission.

980 nm is another pump wavelength to excite Er ions, while in our experiment, the pulley coupler between the bus waveguide and the microdisk cavity is not suitable for efficient coupling of such pump wavelength. Considering the wavelength division of the pump laser and signal laser, a 980 nm pump might be a better choice. The net internal gain of a single spiral waveguide amplifier pumped by a 980 nm laser is larger than that by a 1480 nm laser, which is promising for an integrated device with higher slope efficiency.

We compare the typical parameters of reported work on an Er-doped on-chip laser.[45,48−50,52−60] Our device exhibits the most balanced performance considering the compactness, output laser power, slope efficiency, and linewidth by applying the amplifier-assisted laser design. For further improvement in those figures of merit, multiple methods could be applied. The efficiency could be higher by codoping with Ytterbium ions. Bidirectional pumping could achieve larger output laser power. Optimization of the dry etching would result in a higher loaded quality factor and narrower linewidth.

In summary, by integrating a microdisk cavity with a spiral waveguide on Er-doped TFLN, we demonstrate an efficient on-chip light source with high on-chip laser power (7.989 μW with a nontunable pump), high slope efficiency (0.43% with tunable pump), and narrow linewidth (47.86 kHz with tunable pump). The performance of our device is characterized thoroughly and shows superiority over the conventional microcavity laser. By applying thermal control is applied, a tunable laser is obtained, and a single mode lasing is observed. The device has the potential to be monolithically integrated with other functional devices to form a complete PIC. The improved efficiency also provides a solution for quantum applications. By selective doping, the absorption loss brought by Er ions could be avoided, and by efficient on-chip filtering, the signal laser could propagate to the following devices for modulating, frequency-doubling, or other applications.

METHOD

Device Fabrication. The device is fabricated on a 1-mol % Z-cut Er-doped TFLN with 600 nm thick Er-doped LN (Er:LN), 2-μm-thick silica (SiO_2), and 500-μm-thick silicon (Si) substrate. In order to obtain uniform Er ions doping concentration and achieve a better gain effect, we doped Er ions into LN during the crystal growth processes.[45] The brief fabrication processes of the IAL mainly include six steps: (1) a 600 nm thick amorphous silicon was deposited as a hard etching mask; (2) a layer of resist was spin-coated onto the Er:TFLN; (3) the spiral waveguide structure was patterned via electron- beam lithography (EBL); (4) the mask layer patterns was transferred to the Er:LN layer with an Ar^+ plasma etching process; (5) the residual mask was removed by wet etching; and (6) the two edge facets were milled by focused ion beam (FIB). More fabrication details can be found in the Supporting Information.

EXPERIMENTAL SETUP

The experimental setup is shown in the Supporting Information. A tunable or nontunable pump laser at around 1480/1460 nm, a C-band tunable laser, a polarization controller, a waveguide-fiber coupling system, several beam splitters/combiners, and an optical spectrum analyzer are used to characterize the IAL, microdisk laser, and spiral waveguide amplifier. The laser linewidth is obtained through the beat note

https://doi.org/10.1021/acsphotonics.4c00391
ACS Photonics 2024, 11, 2114−2122

signal of the IAL and a C-band tunable laser using an electrical spectrum analyzer.

■ ASSOCIATED CONTENT

Supporting Information

The Supporting Information is available free of charge at https://pubs.acs.org/doi/10.1021/acsphotonics.4c00391.

Properties of the microdisk laser; properties of the amplifier; polarization-dependent emission; fabrication process and mode profile; experimental setup for the L-L relation and linewidth measurement; thermal evolution of cavity resonance and gain profile; simulation of optimum length of amplifier waveguide (PDF)

■ AUTHOR INFORMATION

Corresponding Author

Yuping Chen − *School of Physics and Astronomy, State Key Laboratory of Advanced Optical Communication Systems and Networks, Shanghai Jiao Tong University, Shanghai 200240, China; School of Physics, Ningxia University, Yinchuan 750021, China;* orcid.org/0000-0003-3969-7119; Email: ypchen@sjtu.edu.cn

Authors

Jiangwei Wu − *School of Physics and Astronomy, State Key Laboratory of Advanced Optical Communication Systems and Networks, Shanghai Jiao Tong University, Shanghai 200240, China*

Xiongshuo Yan − *School of Physics and Astronomy, State Key Laboratory of Advanced Optical Communication Systems and Networks, Shanghai Jiao Tong University, Shanghai 200240, China*

Xueyi Wang − *School of Physics and Astronomy, State Key Laboratory of Advanced Optical Communication Systems and Networks, Shanghai Jiao Tong University, Shanghai 200240, China*

Tingge Yuan − *School of Physics and Astronomy, State Key Laboratory of Advanced Optical Communication Systems and Networks, Shanghai Jiao Tong University, Shanghai 200240, China*

Chengyu Chen − *School of Physics and Astronomy, State Key Laboratory of Advanced Optical Communication Systems and Networks, Shanghai Jiao Tong University, Shanghai 200240, China*

Hao Li − *School of Physics and Astronomy, State Key Laboratory of Advanced Optical Communication Systems and Networks, Shanghai Jiao Tong University, Shanghai 200240, China*

Xianfeng Chen − *School of Physics and Astronomy, State Key Laboratory of Advanced Optical Communication Systems and Networks, Shanghai Jiao Tong University, Shanghai 200240, China; Collaborative Innovation Center of Light Manipulations and Applications, Shandong Normal University, Jinan 250358, China;* orcid.org/0000-0002-1301-7448

Complete contact information is available at: https://pubs.acs.org/10.1021/acsphotonics.4c00391

Author Contributions

†J.W. and X.Y. contributed equally to this work.

Funding

This work was supported by the National Natural Science Foundation of China (Grant Nos. 12134009) and SJTU No. 21X010200828.

Notes

The authors declare no competing financial interest.

■ ACKNOWLEDGMENTS

The authors thank Dr. Jin Li and Prof. Chun-Hua Dong from the University of Science and Technology of China for their technical support. The authors thank the Center for Advanced Electronic Materials and Devices (AEMD) of Shanghai Jiao Tong University (SJTU) for its support in device fabrication.

■ REFERENCES

(1) Bradley, J. D.; Pollnau, M. Erbium-doped integrated waveguide amplifiers and lasers. *Laser & Photonics Reviews* **2011**, *5*, 368−403.

(2) Jiang, X.-F.; Zou, C.-L.; Wang, L.; Gong, Q.; Xiao, Y.-F. Whispering-gallery microcavities with unidirectional laser emission. *Laser & Photonics Reviews* **2016**, *10*, 40−61.

(3) Zhang, Q.; Su, R.; Du, W.; Liu, X.; Zhao, L.; Ha, S. T.; Xiong, Q. Advances in small perovskite-based lasers. *Small Methods* **2017**, *1*, No. 1700163.

(4) Zhang, Q.; Li, G.; Liu, X.; Qian, F.; Li, Y.; Sum, T. C.; Lieber, C. M.; Xiong, Q. A room temperature low-threshold ultraviolet plasmonic nanolaser. *Nat. Commun.* **2014**, *5*, 4953.

(5) Cao, Q.-T.; Liu, R.; Wang, H.; Lu, Y.-K.; Qiu, C.-W.; Rotter, S.; Gong, Q.; Xiao, Y.-F. Reconfigurable symmetry-broken laser in a symmetric microcavity. *Nat. Commun.* **2020**, *11*, 1136.

(6) Tang, S.-J.; Dannenberg, P. H.; Liapis, A. C.; Martino, N.; Zhuo, Y.; Xiao, Y.-F.; Yun, S.-H. Laser particles with omnidirectional emission for cell tracking. *Light: Sci. Appl.* **2021**, *10*, 23.

(7) Zhang, Q.; Shang, Q.; Su, R.; Do, T. T. H.; Xiong, Q. Halide perovskite semiconductor lasers: materials, cavity design, and low threshold. *Nano Lett.* **2021**, *21*, 1903−1914.

(8) Zhou, Z.; Ou, X.; Fang, Y.; Alkhazraji, E.; Xu, R.; Wan, Y.; Bowers, J. E. Prospects and applications of on-chip lasers. *Elight* **2023**, *3*, 1.

(9) Zhang, W.; Xie, X.; Hao, H.; Dang, J.; Xiao, S.; Shi, S.; Ni, H.; Niu, Z.; Wang, C.; Jin, K.; Zhang, X.; Xu, X. Low-threshold topological nanolasers based on the second-order corner state. *Light: Sci. Appl.* **2020**, *9*, 109.

(10) Shang, C.; Feng, K.; Hughes, E. T.; Clark, A.; Debnath, M.; Koscica, R.; Leake, G.; Herman, J.; Harame, D.; Ludewig, P.; Wan, Y.; Bowers, J. E. Electrically pumped quantum-dot lasers grown on 300 mm patterned Si photonic wafers. *Light: Sci. Appl.* **2022**, *11*, 299.

(11) Wei, W.-Q.; He, A.; Yang, B.; Wang, Z.-H.; Huang, J.-Z.; Han, D.; Ming, M.; Guo, X.; Su, Y.; Zhang, J.-J.; Wang, T. Monolithic integration of embedded III-V lasers on SOI. *Light: Sci. Appl.* **2023**, *12*, 84.

(12) Alkhazraji, E.; Chow, W. W.; Grillot, F.; Bowers, J. E.; Wan, Y. Linewidth narrowing in self-injection-locked on-chip lasers. *Light: Sci. Appl.* **2023**, *12*, 162.

(13) Remis, A.; Monge-Bartolome, L.; Paparella, M.; Gilbert, A.; Boissier, G.; Grande, M.; Blake, A.; Ofaolain, L.; Cerutti, L.; Rodriguez, J.-B.; Tournié, E. Unlocking the monolithic integration scenario: optical coupling between GaSb diode lasers epitaxially grown on patterned Si substrates and passive SiN waveguides. *Light: Sci. Appl.* **2023**, *12*, 150.

(14) Ma, J.; Zhou, T.; Tang, M.; Li, H.; Zhang, Z.; Xi, X.; Martin, M.; Baron, T.; Liu, H.; Zhang, Z.; Chen, S.; Sun, X. Room-temperature continuous-wave topological Dirac-vortex microcavity lasers on silicon. *Light: Sci. Appl.* **2023**, *12*, 255.

(15) Ferrara, M. A.; Sirleto, L. Integrated Raman laser: a review of the last two decades. *Micromachines* **2020**, *11*, 330.

(16) Dohnalová, K.; Gregorkiewicz, T.; Kusová, K. Silicon quantum dots: surface matters. *J. Phys.: Condens. Matter* **2014**, *26*, No. 173201.

(17) Nikogosyan, D. N. *Nonlinear Optical Crystals: A Complete Survey*; Springer Science & Business Media, 2006; pp 35−53.
(18) Zhang, M.; Wang, C.; Cheng, R.; Shams-Ansari, A.; Lončar, M. Monolithic ultra-high-Q lithium niobate microring resonator. *Optica* **2017**, *4*, 1536−1537.
(19) Boes, A.; Corcoran, B.; Chang, L.; Bowers, J.; Mitchell, A. Status and potential of lithium niobate on insulator (LNOI) for photonic integrated circuits. *Laser Photonics Rev.* **2018**, *12*, No. 1700256.
(20) Lin, J.; Bo, F.; Cheng, Y.; Xu, J. Advances in on-chip photonic devices based on lithium niobate on insulator. *Photonics Research* **2020**, *8*, 1910−1936.
(21) Luo, R.; He, Y.; Liang, H.; Li, M.; Lin, Q. Highly tunable efficient second-harmonic generation in a lithium niobate nanophotonic waveguide. *Optica* **2018**, *5*, 1006−1011.
(22) Ye, X.; Liu, S.; Chen, Y.; Zheng, Y.; Chen, X. Sum-frequency generation in lithium-niobate-on-insulator microdisk via modal phase matching. *Opt. Lett.* **2020**, *45*, 523−526.
(23) Ge, L.; Chen, Y.; Jiang, H.; Li, G.; Zhu, B.; Liu, Y.; Chen, X. Broadband quasi-phase matching in a MgO:PPLN thin film. *Photonics Research* **2018**, *6*, 954−958.
(24) Lin, J.; Xu, Y.; Ni, J.; Wang, M.; Fang, Z.; Qiao, L.; Fang, W.; Cheng, Y. Phase-Matched Second-Harmonic Generation in an On-Chip $LiNbO_3$ Microresonator. *Physical Review Applied* **2016**, *6*, No. 014002.
(25) Lin, J.; Yao, N.; Hao, Z.; Zhang, J.; Mao, W.; Wang, M.; Chu, W.; Wu, R.; Fang, Z.; Qiao, L.; Fang, W.; Bo, F.; Cheng, Y. Broadband quasi-phase-matched harmonic generation in an on-chip monocrystalline lithium niobate microdisk resonator. *Phys. Rev. Lett.* **2019**, *122*, No. 173903.
(26) Li, X.; Ma, J.; Liu, S.; Huang, P.; Chen, B.; Wei, D.; Liu, J. Efficient second harmonic generation by harnessing bound states in the continuum in semi-nonlinear etchless lithium niobate waveguides. *Light: Sci. Appl.* **2022**, *11*, 317.
(27) Wang, C.; Zhang, M.; Chen, X.; Bertrand, M.; Shams-Ansari, A.; Chandrasekhar, S.; Winzer, P.; Lončar, M. Integrated lithium niobate electro-optic modulators operating at CMOS-compatible voltages. *Nature* **2018**, *562*, 101−104.
(28) Li, M.; Ling, J.; He, Y.; Javid, U. A.; Xue, S.; Lin, Q. Lithium niobate photonic-crystal electro-optic modulator. *Nat. Commun.* **2020**, *11*, 4123.
(29) Xu, M.; He, M.; Zhang, H.; Jian, J.; Pan, Y.; Liu, X.; Chen, L.; Meng, X.; Chen, H.; Li, Z.; Xiao, X.; Yu, S.; Yu, S.; Cai, X. High-performance coherent optical modulators based on thin-film lithium niobate platform. *Nat. Commun.* **2020**, *11*, 3911.
(30) Zhu, D.; Chen, C.; Yu, M.; Shao, L.; Hu, Y.; Xin, C.; Yeh, M.; Ghosh, S.; He, L.; Reimer, C.; Neil Sinclair, M. Z.; Franco, N. C.; Wong; Lončar, M. Spectral control of nonclassical light pulses using an integrated thin-film lithium niobate modulator. *Light: Sci. Appl.* **2022**, *11*, 327.
(31) Wan, L.; Yang, Z.; Zhou, W.; Wen, M.; Feng, T.; Zeng, S.; Liu, D.; Li, H.; Pan, J.; Zhu, N.; Liu, W.; Li, Z. Highly efficient acousto-optic modulation using nonsuspended thin-film lithium niobate-chalcogenide hybrid waveguides. *Light: Sci. Appl.* **2022**, *11*, 145.
(32) Wang, C.; Zhang, M.; Yu, M.; Zhu, R.; Hu, H.; Loncar, M. Monolithic lithium niobate photonic circuits for Kerr frequency comb generation and modulation. *Nat. Commun.* **2019**, *10*, 978.
(33) Fang, Z.; Luo, H.; Lin, J.; Wang, M.; Zhang, J.; Wu, R.; Zhou, J.; Chu, W.; Lu, T.; Cheng, Y. Efficient electro-optical tuning of an optical frequency microcomb on a monolithically integrated high-Q lithium niobate microdisk. *Opt. Lett.* **2019**, *44*, 5953−5956.
(34) He, Y.; Yang, Q.-F.; Ling, J.; Luo, R.; Liang, H.; Li, M.; Shen, B.; Wang, H.; Vahala, K.; Lin, Q. Self-starting bi-chromatic $LiNbO_3$ soliton microcomb. *Optica* **2019**, *6*, 1138−1144.
(35) Wang, X.; Yuan, T.; Wu, J.; Chen, Y.; Chen, X. Enhanced Temperature Sensing by Multi-Mode Coupling in an On-Chip Microcavity System. *Laser Photon. Rev.* **2024**, *18* (4), No. 2300760.
(36) Wang, X.; Wu, J.; Chen, C.; Yuan, T.; Chen, Y.; Chen, X. Enhanced sensing resolution with microcavity mode oscillation generated by thermal-optic and photorefractive nonlinearity. *Appl. Phys. Lett.* **2024**, *124*, No. 061108, DOI: 10.1063/5.0188236.
(37) Shams-Ansari, A.; Renaud, D.; Cheng, R.; Shao, L.; He, L.; Zhu, D.; Yu, M.; Grant, H. R.; Johansson, L.; Zhang, M.; Lončar, M. Electrically pumped laser transmitter integrated on thin-film lithium niobate. *Optica* **2022**, *9*, 408−411.
(38) Agazzi, L.; Worhoff, K.; Pollnau, M. Energy-transfer-upconversion models, their applicability and breakdown in the presence of spectroscopically distinct ion classes: A case study in amorphous Al_2O_3: Er^{3+}. *J. Phys. Chem. C* **2013**, *117*, 6759−6776.
(39) Mu, J.; Dijkstra, M.; Korterik, J.; Offerhaus, H.; García-Blanco, S. M. High-gain waveguide amplifiers in Si_3N_4 technology via double-layer monolithic integration. *Photonics Research* **2020**, *8*, 1634−1641.
(40) Rönn, J.; Zhang, J.; Zhang, W.; Tu, Z.; Matikainen, A.; Leroux, X.; Durán-Valdeiglesias, E.; Vulliet, N.; Boeuf, F.; Alonso-Ramos, C.; Lipsanen, H.; Vivien, L.; Sun, Z.; Cassan, E. Erbium-doped hybrid waveguide amplifiers with net optical gain on a fully industrial 300 mm silicon nitride photonic platform. *Opt. Express* **2020**, *28*, 27919−27926.
(41) Vázquez-Córdova, S. A.; Dijkstra, M.; Bernhardi, E. H.; Ay, F.; Wörhoff, K.; Herek, J. L.; García-Blanco, S. M.; Pollnau, M. Erbium-doped spiral amplifiers with 20 dB of net gain on silicon. *Opt. Express* **2014**, *22*, 25993−26004.
(42) Rönn, J.; Zhang, W.; Autere, A.; Leroux, X.; Pakarinen, L.; Alonso-Ramos, C.; Säynätjoki, A.; Lipsanen, H.; Vivien, L.; Cassan, E.; Sun, Z. Ultra-high on-chip optical gain in erbium-based hybrid slot waveguides. *Nat. Commun.* **2019**, *10*, 432.
(43) Min, B.; Kippenberg, T. J.; Yang, L.; Vahala, K. J.; Kalkman, J.; Polman, A. Erbium-implanted high-Q silica toroidal microcavity laser on a silicon chip. *Phys. Rev. A* **2004**, *70*, No. 033803.
(44) Li, H.; Wang, Z.; Wang, L.; Tan, Y.; Chen, F. Optically pumped milliwatt whispering-gallery microcavity laser. *Light: Sci. Appl.* **2023**, *12*, 223.
(45) Liu, Y.; Yan, X.; Wu, J.; Zhu, B.; Chen, Y.; Chen, X. On-chip erbium-doped lithium niobate microcavity laser. *Sci. China: Phys., Mech. Astron.* **2021**, *64*, No. 234262.
(46) Jia, Y.; Wu, J.; Sun, X.; Yan, X.; Xie, R.; Wang, L.; Chen, Y.; Chen, F. Integrated Photonics Based on Rare-Earth Ion-Doped Thin-Film Lithium Niobate. *Laser Photonics Rev.* **2022**, *16*, No. 2200059.
(47) Chen, Y. Photonic integration on rare earth ion-doped thin-film lithium niobate. *Sci. China: Phys., Mech. Astron.* **2022**, *65*, No. 294231, DOI: 10.1007/s11433-022-1945-4.
(48) Yin, D.; Zhou, Y.; Liu, Z.; Wang, Z.; Zhang, H.; Fang, Z.; Chu, W.; Wu, R.; Zhang, J.; Chen, W.; Wang, M.; Cheng, Y. Electro-optically tunable microring laser monolithically integrated on lithium niobate on insulator. *Opt. Lett.* **2021**, *46*, 2127−2130.
(49) Wang, Z.; Fang, Z.; Liu, Z.; Chu, W.; Zhou, Y.; Zhang, J.; Wu, R.; Wang, M.; Lu, T.; Cheng, Y. On-chip tunable microdisk laser fabricated on Er^{3+}-doped lithium niobate on insulator. *Opt. Lett.* **2021**, *46*, 380−383.
(50) Luo, Q.; Hao, Z.; Yang, C.; Zhang, R.; Zheng, D.; Liu, S.; Liu, H.; Bo, F.; Kong, Y.; Zhang, G.; Xu, J. Microdisk lasers on an erbium-doped lithium-niobate chip. *Sci. China: Phys., Mech. Astron.* **2021**, *64*, No. 234263.
(51) Luo, Q.; Yang, C.; Zhang, R.; Hao, Z.; Zheng, D.; Liu, H.; Yu, X.; Gao, F.; Bo, F.; Kong, Y.; Zhang, G.; Xu, J. On-chip erbium-doped lithium niobate microring lasers. *Opt. Lett.* **2021**, *46*, 3275−3278.
(52) Liu, X.; Yan, X.; Liu, Yian; Li, H.; Chen, Y.; Chen, X. Tunable single-mode laser on thin film lithium niobate. *Opt. Lett.* **2021**, *46*, 5505−5508.
(53) Gao, R.; Guan, J.; Yao, N.; Deng, L.; Lin, J.; Wang, M.; Qiao, L.; Wang, Z.; Liang, Y.; Zhou, Y.; Cheng, Y. On-chip ultra-narrow-linewidth single-mode microlaser on lithium niobate on insulator. *Opt. Lett.* **2021**, *46*, 3131−3134.
(54) Zhang, R.; Yang, C.; Hao, Z.; Jia, D.; Luo, Q.; Zheng, D.; Liu, H.; Yu, X.; Gao, F.; Bo, F.; YongFa Kong, G. Z.; Xu, J. Integrated lithium niobate single-mode lasers by the Vernier effect. *Sci. China: Phys., Mech. Astron.* **2021**, *64*, No. 294216.

(55) Xiao, Z.; Wu, K.; Cai, M.; Li, T.; Chen, J. Single-frequency integrated laser on erbium-doped lithium niobate on insulator. *Opt. Lett.* **2021**, *46*, 4128−4131.
(56) Li, T.; Wu, K.; Cai, M.; Xiao, Z.; Zhang, H.; Li, C.; Xiang, J.; Huang, Y.; Chen, J. A single-frequency single-resonator laser on erbium-doped lithium niobate on insulator. *APL Photonics* **2021**, *6*, No. 101301.
(57) Lin, J.; Farajollahi, S.; Fang, Z.; Yao, N.; Gao, R.; Guan, J.; Deng, L.; Lu, T.; Wang, M.; Zhang, H.; Fang, W.; Qiao, L.; Cheng, Y. Electro-optic tuning of a single-frequency ultranarrow linewidth microdisk laser. *Advanced Photonics* **2022**, *4*, No. 036001.
(58) Liang, Y.; Zhou, J.; Wu, R.; Fang, Z.; Liu, Z.; Yu, S.; Yin, D.; Zhang, H.; Zhou, Y.; Liu, J.; Wang, Z.; Wang, M.; Cheng, Y. Monolithic single-frequency microring laser on an erbium-doped thin film lithium niobate fabricated by a photolithography assisted chemo-mechanical etching. *Optics Continuum* **2022**, *1*, 1193−1201.
(59) Zhu, Y.; Zhou, Y.; Wang, Z.; Fang, Z.; Liu, Z.; Chen, W.; Wang, M.; Zhang, H.; Cheng, Y. Electro-optically tunable microdisk laser on Er^{3+}-doped lithium niobate thin film. *Chinese Optics Letters* **2022**, *20*, No. 011303.
(60) Guan, J.; Li, C.; Gao, R.; Zhang, H.; Lin, J.; Li, M.; Wang, M.; Qiao, L.; Deng, L.; Cheng, Y. Monolithically integrated narrow-bandwidth disk laser on thin-film lithium niobate. *Optics & Laser Technology* **2024**, *168*, No. 109908.
(61) Yu, S.; Fang, Z.; Wang, Z.; Zhou, Y.; Huang, Q.; Liu, J.; Wu, R.; Zhang, H.; Wang, M.; Cheng, Y. On-chip single-mode thin-film lithium niobate Fabry-Perot resonator laser based on Sagnac loop reflectors. *Opt. Lett.* **2023**, *48*, 2660−2663.
(62) Zhou, Y.; et al. Monolithically Integrated Active Passive Waveguide Array Fabricated on Thin Film Lithium Niobate Using a Single Continuous Photolithography Process. *Laser Photonics Rev.* **2023**, *17*, No. 2200686.
(63) Yan, X.; Liu, Y.; Wu, J.; Chen, Y.; Chen, X. Integrated spiral waveguide amplifiers on erbium-doped thin-film lithium niobate. *arXiv* **2021**, 2105.00214.
(64) Zhou, J.; Liang, Y.; Liu, Z.; Chu, W.; Zhang, H.; Yin, D.; Fang, Z.; Wu, R.; Zhang, J.; Chen, W.; Wang, Z.; Zhou, Y.; Wang, M.; Cheng, Y. On-chip integrated waveguide amplifiers on erbium-doped thin-film lithium niobate on insulator. *Laser Photonics Rev.* **2021**, *15*, No. 2100030.
(65) Chen, Z.; Xu, Q.; Zhang, K.; Wong, W.-H.; Zhang, D.-L.; Pun, E. Y.-B.; Wang, C. Efficient erbium-doped thin-film lithium niobate waveguide amplifiers. *Opt. Lett.* **2021**, *46*, 1161−1164.
(66) Luo, Q.; Yang, C.; Hao, Z.; Zhang, R.; Zheng, D.; Bo, F.; Kong, Y.; Zhang, G.; Xu, J. On-chip erbium-doped lithium niobate waveguide amplifiers. *Chinese Optics Letters* **2021**, *19*, No. 060008.
(67) Liang, Y.; Zhou, J.; Liu, Z.; Zhang, H.; Fang, Z.; Zhou, Y.; Yin, D.; Lin, J.; Yu, J.; Wu, R.; Wang, M.; Cheng, Y. A high-gain cladded waveguide amplifier on erbium doped thin-film lithium niobate fabricated using photolithography assisted chemo-mechanical etching. *Nanophotonics* **2022**, *11*, 1033−1040.
(68) Zhang, Z.; Fang, Z.; Zhou, J.; Liang, Y.; Zhou, Y.; Wang, Z.; Liu, J.; Huang, T.; Bao, R.; Yu, J.; Zhang, H.; Wang, M.; Cheng, Y. On-chip integrated Yb^{3+}-doped waveguide amplifiers on thin film lithium niobate. *Micromachines* **2022**, *13*, 865.
(69) Cai, M.; Wu, K.; Xiang, J.; Xiao, Z.; Li, T.; Li, C.; Chen, J. Erbium-doped lithium niobate thin film waveguide amplifier with 16 dB internal net gain. *IEEE J. Sel. Top. Quantum Electron.* **2022**, *28*, 1−8.
(70) Saravi, S.; Pertsch, T.; Setzpfandt, F. Lithium niobate on insulator: An emerging platform for integrated quantum photonics. *Adv. Opt. Mater.* **2021**, *9*, No. 2100789.
(71) Yang, L.; Wang, S.; Shen, M.; Xie, J.; Tang, H. X. Controlling single rare earth ion emission in an electro-optical nanocavity. *Nat. Commun.* **2023**, *14*, 1718.
(72) Xia, K.; Sardi, F.; Sauerzapf, C.; Kornher, T.; Becker, H.-W.; Kis, Z.; Kovacs, L.; Dertli, D.; Foglszinger, J.; Kolesov, R.; Wrachtrup, J. Tunable microcavities coupled to rare-earth quantum emitters. *Optica* **2022**, *9*, 445−450.
(73) Saglamyurek, E.; Sinclair, N.; Jin, J.; Slater, J. A.; Oblak, D.; Bussieres, F.; George, M.; Ricken, R.; Sohler, W.; Tittel, W. Broadband waveguide quantum memory for entangled photons. *Nature* **2011**, *469*, 512−515.
(74) Sinclair, N.; Heshami, K.; Deshmukh, C.; Oblak, D.; Simon, C.; Tittel, W. Proposal and proof-of-principle demonstration of non-destructive detection of photonic qubits using a Tm: $LiNbO_3$ waveguide. *Nat. Commun.* **2016**, *7*, No. 13454.
(75) Sinclair, N.; Oblak, D.; Thiel, C. W.; Cone, R. L.; Tittel, W. Properties of a rare-earth-ion-doped waveguide at sub-kelvin temperatures for quantum signal processing. *Physical review letters* **2017**, *118*, No. 100504.
(76) Zhang, X.; Zhang, B.; Wei, S.; Li, H.; Liao, J.; Li, C.; Deng, G.; Wang, Y.; Song, H.; You, L.; Jing, B.; Chen, F.; Guo, G.; Zhou, Q. Telecom-band−integrated multimode photonic quantum memory. *Sci. Adv.* **2023**, *9*, No. eadf4587.
(77) Huang, C.-h.; McCaughan, L.; Gill, D. M. Evaluation of absorption and emission cross sections of Er-doped $LiNbO_3$ for application to integrated optic amplifiers. *J. Lightwave Technol.* **1994**, *12*, 803−809.

https://doi.org/10.1021/acsphotonics.4c00391
ACS Photonics 2024, 11, 2114−2122